Fracture stability and Micromechanics of Strain Hardening Cementitious Composites

L.G. Sorelli & F.-J. Ulm
Massachusetts Institute of Technology, Cambridge, USA

F. Toutlemonde
Laboratoire des Ponts et Chaussées, Paris, France

ABSTRACT: Innovative cementitious composites endowed with strain hardening behavior, namely UHPFRC, have been successfully employed in several industrial applications, such as bridge engineering and nuclear waste container prototypes, where the crack impact on the durability is of main concern. However, the material ductility of such composites exhibits a complex dependence on the fiber distribution that has been an important issue in the design recommendations (AFGC, 2002). In this paper, we develop an approximate energy-balance approach to link the overall damage to non-uniform fiber distribution. The thermodynamics principles and the micromechanics based secant stiffness formulation allowed us to derive the non linear constitutive stress-strain relationship of the material from the fiber distribution and properties of the composite phases. Finally, the model implication on the stability of the post-cracking behavior is discussed together with an example of industrial application for nuclear waste container.

1 INTRODUCTION

In the last decade, several structural applications of Ultra High Performance Fiber Reinforced Composite (UHPFRC) have been emerging in bridge engineering, rehabilitation and strengthening techniques of damaged structures, nuclear waste container, etc. The driving force of these new materials is the optimized microstructure that has been tailored to achieve high durability, ultra high compressive strength, and tensile pseudo-hardening behavior (Chanvillard & Rigaud, 2003). However, design codes require a reliable assessment of the post-cracking ductility and fracture energy, especially in relation to the microstructure variability. For example, the first design recommendations for UHPFRC (AFGC, 2002) reduces the characteristic tensile law of bended standard specimens by a factor (K = 1.25-1.75) to account for the effective fiber distribution within the structure. Moreover, structural applications have been limited to thin elements where the fiber distribution is favored by wall effects (e.g., the fiber efficiency, defined as the average fiber projection in the direction of the external load, is $2/\pi$ and $1/2$ for 2D and 3D random distribution, respectively).

The importance of the fiber distribution on the mechanical properties has been verified experimentally (Bernier & Behloul, 1998; Bayard & Plé, 2003; Chanvillard & Rigaud, 2003). For example, uniaxial tests on UHPFRC blocks reinforced with five differ-

ent fiber orientations showed the first crack occurs almost always perpendicular to the loading axis regardless the fiber distribution (Bayard & Plé, 2003). Remarkably, the fracture energy reduces by a factor of about four when the fiber alignment changes from 0º to 90º. As for the flexural behavior, the post-cracking response of beams strongly depends on the fiber orientation up to an extent that, when the fibers are unfavorably aligned (e.g., parallel to the major crack direction), the material does not exhibit strain hardening behavior (Bernier & Behloul, 1998).

At observation scale below macroscopic testing, the cracks initiate on a very small length scale within the cementitious matrix, and they evolve into fiber-matrix interface failure. Remarkably, a weak fiber-matrix interface may favor high toughness by promoting fiber-matrix interface failure (Marshall & Cox, 1985; Leung, 1996; Lin & Li, 1997). Moreover, other micromechanics phenomena may be at stake, such as matrix crumbling at the fiber exit point (Zhang & Li, 2002), local fiber bending and yielding (Leung & Chi, 1995), and fiber rupture.

Chuang *et al.* (2001) showed that, in UHPFRC materials, the fiber aspect ratio (i.e., the length-to-diameter ratio of the fiber) is optimally designed to induce simultaneous fiber debonding and matrix cracking. Contrarily, in normal FRC, the fiber length is often insufficient to satisfactory prevent early interface failure and the average fiber distance is too large to lead to multiple cracking (i.e., the fiber is over designed with respect to the matrix strength).

Energy based approaches have been a powerful analytical tool to study fiber reinforced composites. Budiansky et al. (1986) applied a variational energy approach to study fiber-matrix interface failure showing that, in case of initially bonded fibers, a fairly small interface debonding toughness suffices to inhibit crack localization. Energy approaches have been also employed to identify the necessary conditions for the strain hardening: (i) the complementary energy has to exceed the crack tip resistant energy at the steady state crack propagation (Marshall & Cox, 1985); (ii) the first cracking strength should be lower than the maximum composite fiber strength (Leung, 1996). By comparing the energy to form a new crack with the energy to open the first formed crack, Tjiptobroto and Hansen (1993) proposed an analytical expression for the strain at the end of multiple cracking.

Recently, continuum micromechanics theories have allowed disclosing the link between the microstructure and the overall properties. Karihaloo et al. (1996) accounted for the interaction of microcrack distribution by solving the elastic problem of a doubly periodic array of elastically bridged cracks. However, experimental fracture tests indicate the crack distribution is random in nature. Dormieux et al. (2006) developed a fracture-micromechanics approach to model interacting random microcracks in presence of internal fluid pressure. Notably, they found that crack interaction may be a reason of strain softening behavior and that the energetic stability depends on the initial critical crack size and fracture energy.

In this work, we pursue an energy based approach that derives the constitutive macro stress-strain relationship of UHPFRC materials from their critical microstructure features (i.e., the fiber distribution and the distribution of interacting cracks). However, at this first approach stage, we will focus only on the strain hardening phase, while disregarding the subsequent crack localization.

2 A FRACTURE-MICROMECHANICS APPROACH

Every structural system can be characterized by a length scale L defining the structural dimension. At a level below, we consider a material point of elementary volume, which includes sufficient matter to be representative and it is characterized by a macroscopic length scale D. Below this scale, the matter is heterogeneous and this material system is characterized by the scale d of its components at the microscopic level (for instance, the grain diameter or the aggregate size). A continuum description of a heterogeneous material requires that characteristic length (D) has to be much larger than dimension (d) of the components and much smaller than the struc-

tural dimensions (L). Figure 1 shows the qualitative multi-scale approach adopted in this work for describing a UHPFRC composite materials made of three phases, namely the discontinuous steel fibers, penny-shaped cracks, and the cement-based matrix.

In the following, we assume a micros-scale system made of an elastic-brittle matrix with narrow (or penny-shaped) cracks, while the fiber is indirectly only considered in term of the energetic contribution to delay the crack propagation. However, the fiber energy is linked to the fiber-matrix interface micromechanics and the fiber orientation distribution. This approximation disregards the effect of fiber on the elastic properties of the bulk material, which is expected to be limited for the considered UHPFRC fiber content (Chanvillard & Rigaud, 2003).
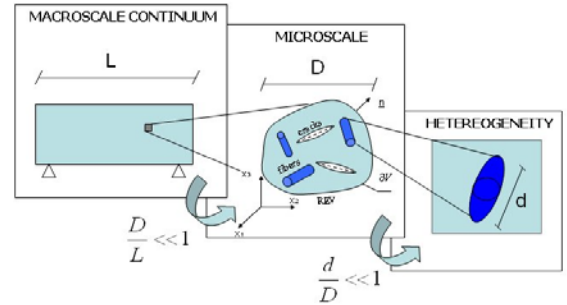

Figure 1. Multi-scale approach for UHPFRC materials.

2.1 Thermodynamics of an elastic cracked medium

The simplest crack system of a single planar crack embedded in an unbounded linear elastic material is analyzed within the theoretical framework of classical thermodynamics, Dormieux et al. (2006). The incremental externally supplied work δW^{ext} provided to the solid Ω is stored in form of elastic energy density $\Omega_0 d\psi$ in the solid (where Ω_0 denotes the initial volume of the considered structure and ψ the elastic free energy density of the solid part). Our starting point is the Clausius-Duhem inequality which states that the externally supplied work to the solid (δW^{ext}), which is not stored as free energy $\Omega_0 d\psi$ (or Helmholtz energy) in the system, is dissipated into heat

$$dD = \delta W^{ext} - \Omega_0 d\psi \geq 0 \qquad (1)$$

The externally supplied work δW^{ext} is related to the surface forces T acting on the incremental displacement $d\xi$ over the external surface $\partial\Omega$ (i.e., body force are neglected) as follows

$$\delta W^{ext} = \int_{\partial\Omega} T \cdot d\xi \, dS \qquad (2)$$

We now express the free energy elastic of the solid matrix $\Psi = \Psi(E, \ell)$ as a macro-potential function of two variables, such as the elastic strain E (observable variable) and the crack area ℓ (state variable). In the case of reversible evolutions $dD = 0$, ℓ is constant. By contrast, when the crack propagates,

the free energy changes not only with the incremental strain dE, but as well due to the increase of fracture surface ℓ. Introducing (2) into (1), we obtain

$$dD = \left(\int_{\partial\Omega} T \cdot d\xi \, dS - \Omega_0 \frac{\partial \psi}{\partial E} dE \right) - \Omega_0 \frac{\partial \psi}{\partial \ell} d\ell \geq 0 \quad (3)$$

Fracture propagation dissipates energy through creation of additional crack surface $d\ell$ and the dissipation rate is evaluated from Eq. (3)

$$dD = -\Omega_0 \left(\frac{\partial \Psi(E,\ell)}{\partial \ell} \right)_{dE=0} d\ell = G_A(E,\ell) \, d\ell \geq 0 \quad (4)$$

Remarkably, Eq.(4) indicates that the thermodynamic driving force of the crack propagation is the energy release $G_A(E,\ell)$. For example, in the case of a Griffith's crack a fast run crack propagates, in an unstable manner, when the energy release rate $G_A(\ell)$ reaches a critical threshold (R_0), which is called *fracture energy* and is often considered a material property. Owing the linearity of the solid behavior, the free energy is expected to be a quadratic function of E and Σ:

$$\Psi(E,\ell) = \frac{1}{2} E : C^{\text{hom}}(\ell) : E \quad (5)$$

Introducing the above equation in (3) allows us to identify the state equations of the cracked medium:

$$\Sigma = \frac{\partial \psi}{\partial E} = C^{\text{hom}}(\ell) : E \quad (6)$$

Now, Eq. (4) takes the form

$$G_A = \frac{\partial \psi(E,\ell)}{\partial \ell} = -\frac{1}{2} E : \frac{\partial C^{\text{hom}}(\ell)}{\partial \ell} : E \geq 0 \quad (7)$$

The energy release G_A can be estimated from the homogenized secant stiffness in function of the geometric parameter ℓ.

The approach of Dormiuex *at al.* (2006) can be extended to account the energy contribution of the fiber bridged zone behind the crack tip, we can employ the J-Rice integral, which is an alternative and convenient mathematically form of the energy conservation principle. Thus, the crack energy release can be computed as follows

$$J_B = \oint (\psi \, n_1 + \frac{\partial [\![\xi]\!]}{\partial x_1}) \, dS = \int_\lambda^L \sigma([\![\xi]\!])(\partial [\![\xi]\!]/\partial x) \, dx =$$
$$= -\int_0^{[\![\xi]\!]} \sigma([\![\xi]\!]) \, d[\![\xi]\!] = G_B \quad (8)$$

where $[\![\xi]\!]$ is the crack opening displacement and $\sigma([\![\xi]\!])$ is the fiber bridging stress across the crack surfaces. We emphasize that the fiber energy can be seen as an energy release (G_B) or a toughness term (R_B) depending on the observer's frame. In this case, an observer on the crack enclave will perceive the

fiber as applied external forces. Figure 2 qualitatively shows the J-Rice integral contours around the fiber bridged crack.
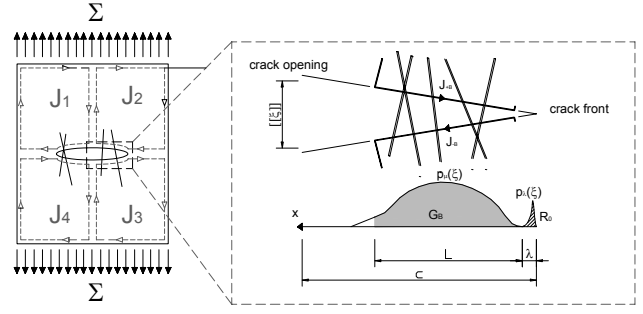

Figure 2. J-Rice integral contours along bridged crack surfaces with enlarged view (right) of the stress-separation function $p_u([\![\xi]\!])$.

The presence of two system of loads (i.e., external loads and fibers bridging force) involves additional energy cross-terms, which come from the energy release of the strain energy stored through the indirect work. Although the energy releases are not additive, they are square root additive (Bažant & Planas, 1998), because of the Irwin relationship $G=K^2/E$' between the energy release G and the stress intensity factor K. Hence, the energy balance equation (4) can be written as

$$dD = R_0 = G_A + G_B + 2\sqrt{G_A}\sqrt{G_B} \geq 0 \quad (9)$$

We can define the loading function

$$f(E,\ell) = \Sigma_i G_i(E,\ell) - R_0 \quad (10)$$

which can be used to mathematically describe the loading/unloading conditions:

$$f(\ell) \leq 0, \quad f(\ell) \, d\ell = 0, \quad d\ell \geq 0 \quad (11)$$

If, due to incremental fracture propagation $\ell \to \ell + d\ell$, the energy release decreases from $\Sigma_i G_i(E,\ell) = R(E,\ell)$ to $\Sigma_i G_i(E,\ell+d\ell) < R_0$, the crack propagation will stop. This corresponds to stable fracture propagation if

$$\frac{\partial f}{\partial \ell} = \Sigma_i \left(\frac{\partial G_i(E,\ell)}{\partial \ell} \right)_{dE=0} < 0 \quad (12)$$

or otherwise unstable. In the following, we determine the terms of energy equation (9) from micromechanics theory.

2.2 *Micromechanics background*

The premises of homogenization theory are that the macroscopic stress and strain quantities (Σ, E) are volume averages of local stress and strain (σ, ε) quantities:

$$\Sigma = \langle \sigma \rangle = \frac{1}{\Omega} \int_\Omega \sigma(x) d\Omega; \quad E = \langle \varepsilon \rangle = \frac{1}{\Omega} \int_\Omega \varepsilon(x) d\Omega \quad (13)$$

where the angular bracket stand simply for the spatial average phase average operator such as

$$\langle b \rangle = \frac{1}{\Omega} \int b \, d\Omega \tag{14}$$

Uniform internal strain is possible only if the material is homogeneous. For uniform boundary condition, the applied strain E on the surface $\partial\Omega$, subjected to a displacement ξ^d, reads

$$\xi^d = E \cdot z \quad \vee z \in \partial\Omega \tag{15}$$

where z = the local coordinate system. Some simplifications in the geometrical description are usually necessary to deal with complex microstructure interactions. First, we assume that each rth phase is linear elastic with isotropic stiffness tensor C_r, and the following constitutive relation holds for each phase

$$\sigma(z_r) = C_r : \varepsilon(z_r) \tag{16}$$

The strain fields within the rth constituent is approximated by their phase average, and it is linked to the macroscopic strain by a linear strain localization tensors A_r

$$\overline{\varepsilon}_r = \langle \varepsilon \rangle_r = A_r : \langle \varepsilon \rangle = A_r : E \tag{17}$$

The overall stress Σ can be expressed in terms of the average strain of each rth phase as follows

$$\Sigma = C^{\text{hom}} : E = \sum_{r=0}^{N} f_r \langle \sigma_r \rangle_{(r)} = \sum_{r=0}^{N} f_r A_r : E \tag{18}$$

which, after simple mathematical manipulations, leads to the composite stiffness

$$C^{\text{hom}} = \sum_{r=0}^{N} f_r C_r : A_r \tag{19}$$

Note that the summation of the strain localizer or stress tensor over all the phases gives the identity matrix (i.e., compatibility condition):

$$\sum_{r=0}^{N} f_r A_r = I \tag{20}$$

Inserting the Eq. (20) into (19), we obtain the following simplified relation:

$$C^{\text{hom}} = C_0 + \sum_{r=1}^{N} f_r (C_r - C_0) : A_r \tag{21}$$

We remark that, although several homogenization models have these previous steps in common, they differ for the localizer tensor A_r that represents the effect of the morphology microstructure. For example, the dilute scheme assumes a single inclusion embedded in an unbounded medium with elastic modulo C_0 of the matrix, i.e., the inclusion interactions are neglected. The strain localization tensor reads

$$A_r^{Esh} = [I + S_r C_0^{-1}(C_r - C_0)]^{-1} \tag{22}$$

where S_r is the Eshelby tensor analytically derived from the problem of a constant strain within an ellipsoidal inclusion body (Eshelby, 1957).

To account for interactions between the inclusions, we will use the Mori-Tanaka (1973) homogenization scheme that considers a single inclusion embedded in a reference material with the average strain of the matrix. The Mori-Tanaka estimate is relevant for morphology of microstructure where the cavity can be regarded as inclusions embedded in a continuum matrix, and its strain concentration tensor reads:

$$A_r^{MT} = [I + S_r C_0^{-1}(C_r - C_0)]^{-1} : \langle I + S_r C_0^{-1}(C_r - C_0) \rangle^{-1} \tag{23}$$

We statistically describe a network of microcracks by the joint probability density distribution $f(a, \vartheta, \varphi)$ of the crack sizes and orientations (where ϑ, φ are two Euler angles describing the crack orientation). Its integral on a sphere of unit radius gives the volume of crack per unit volume N such as

$$N = \frac{1}{4\pi} \int_{a=a_{\min}}^{a_{\max}} \int_{\varphi=0}^{2\pi} \int_{\vartheta=0}^{\pi} f(a, \vartheta, \varphi) \sin\vartheta \, da \, d\vartheta \, d\varphi \tag{24}$$

Assuming that the crack size distribution is independent of the crack orientation, the density distribution simplifies as $f(a, \vartheta, \varphi) = f_a(a)f_r(\vartheta, \varphi)$ and it follows

$$a = \int_{a=a_{\min}}^{a_{\max}} f_o(a) da$$
$$N = \frac{1}{4\pi} \int_{\varphi=0}^{2\pi} \int_{\vartheta=0}^{\pi} f(\vartheta, \varphi) \sin\vartheta \, d\vartheta \, d\varphi \tag{25}$$

We define a crack family composed by penny-shaped cracks with the same orientation (n) and crack radius (surface area $\ell = \pi a^2$, crack density N). Moreover, for each crack family, it is convenient to introduce the micromechanics damage parameter $\epsilon = Na^3$, defined by Budiansky et al. (1976). Hence, the crack volume fraction (f_c) of N penny-shaped crack can be expressed in terms of the micromechanical damage density parameter as follows

$$f_c = N \frac{4}{3} \pi a^3 X = \frac{4}{3} \pi \epsilon X \tag{26}$$

where the crack aspect ratio X = c / a has been used in the ellipsoid volume formula. For example, in the case of a system of microcracks and a solid matrix, relation (26) into (21) yields

$$C^{\text{hom}} = C_0 : (I - f_c A_c) = C_0 : (I - \frac{4}{3}\pi\epsilon X A_c) =$$
$$= C_0 : (I - \frac{4}{3}\pi\epsilon T(\underline{n})) \tag{27}$$

where the tensor T has the property to have a finite limit when $X \rightarrow 0$ such as

$$T = \lim_{x \to 0} X(I - S_{ps}(X, \underline{n}))^{-1} \qquad (28)$$

3 NON LINEAR FRACTURE MECHANICS

In a quasi-static fracture process (without inertia forces), the energy equality $\Sigma G = \Sigma R$ is satisfied whenever the crack is growing. Following the "R-curve" approach (Bažant and Planas, 1998), we analyze a tensile test under mode-I condition by solving the system of the energy balance equation and the (macro) stress-strain relations based on the secant stiffness:

$$f(\epsilon, E) = \sum_i G_i(\epsilon, E) - R(\epsilon) = 0 \qquad (29)$$
$$\Sigma = C(\epsilon) : E$$

For numerical implementation it is convenient to cast the Eq. (29) in a rate form and to derive the tangent stiffness between the macro-stress (Σ) and macro-strain (E). When the crack grows ($d\epsilon \neq 0$), the condition df = 0 can be re-written as

$$df(\epsilon, E) = \frac{\partial f}{\partial \epsilon} d\epsilon + \frac{\partial f}{\partial E} dE = 0 \rightarrow \frac{d\epsilon}{dE} = -\frac{\partial f / \partial E}{\partial f / \partial \epsilon} \qquad (30)$$

Then, the tangent material stiffness at the beginning of each loading increment $d\Sigma$ (or strain increment dE) can be formulated in terms of known quantities in an explicit manner such as

$$\frac{d\Sigma}{dE} = C(\epsilon) + \frac{\partial C(\epsilon)}{\partial \epsilon} \frac{\partial \epsilon}{\partial E} = C(\epsilon) - \frac{\partial C(\epsilon)}{\partial \epsilon} \frac{\partial f / \partial E}{\partial f / \partial \epsilon} \qquad (31)$$

Before solving Eq. (29), we need to define the fracture energy R_0 and the fiber energy G_B in terms of the microstructure crack density parameter ϵ, which is the loading history parameter. Again disregarding fracture energy interaction, the total dissipation is the sum of the contributions of all the N cracks which are assumed to propagate of the same amount $d\ell$. For simplicity, we assume the crack grows simultaneously with constant number N in order that ℓ and ϵ are equivalent state variables (in accordance with Dormieux *et al.*, 2006):

$$\ell = \pi \left(\frac{\epsilon}{N} \right)^{2/3} ; \quad d\ell = \frac{2\pi}{3N^{2/3}} \epsilon^{-1/3} d\epsilon$$

The elementary contribution of a single crack to the total dissipation is given by

$$R_0 \, d\ell = N \, Gf \, d\ell = R_{0\epsilon} d\epsilon \qquad (32)$$

where

$$R_{0\epsilon} = \frac{2\pi}{3} G_f \left(\frac{N}{\epsilon} \right)^{1/3} = \frac{2\pi}{3} \frac{G_f}{a} \qquad (33)$$

Hence, after this change of variable, R_0 is not anymore an independent variable but is dependent on the crack size, and hence on the loading history. We are now left to find the fiber energy term G_B of equation (29). We will address this point in the following section adopting a statistical fiber distribution.

4 FIBER DEBONDING ENERGY

This section reviews the analytical model for fiber-matrix micromechanics proposed by Lin and Li (1997), which extends the previous work of Marshall & Cox (1985). The constitutive relation between the fiber pull-out force (F) and the crack opening displacement ($[[\xi]]$) holds the key of the underlying role of the fiber micro-mechanisms and several authors (Marshall & Cox, 1985; Li & Leung, 1992; Lin & Li, 1997) have proposed the following form:

$$F_d \left([[\xi]] \right) = k [[\xi]]^{1/2} \qquad if \; [[\xi]] \leq [[\xi]]^*$$
$$F_s \left([[\xi]] \right) = k \frac{[[\xi]]^{cr} - [[\xi]]}{[[\xi]]^{cr} - [[\xi]]^*} \qquad if \; [[\xi]]^* \leq [[\xi]] \leq [[\xi]]^{cr} \qquad (34)$$

where the load coefficient and the crack opening thresholds are defined as

$$k = \frac{1}{2} \pi \, \phi_f \sqrt{(1+\eta) \tau_u E_f \phi_f} ; \quad \eta = \frac{E_f V_f}{E_m V_m}$$
$$[[\xi]]^* = \frac{4(1+\eta)\tau_u L_f^{\,2}}{E_f \phi_f}; \quad [[\xi]]^{cr} = L_f / 2 \qquad (35)$$

where E_f and E_m are the elastic modulus of fiber and matrix, respectively; L_f = fiber length; ϕ_f = fiber diameter; and τ_u = fiber-matrix frictional debonding. The model parameters employed in this work are summarized in Table 1.

Experimental pull-out tests of steel micro-fibers showed that the effect of matrix edge pulley and the fiber local moment tend approximately to compensate each other over the possible fiber inclinations (Shah and Ouyang, 1991). For simplicity, the fiber orientation effect on the pull-out response of a single fiber is here neglected.

Table 1. Fiber-matrix interface model parameters.

E_m [GPa]	E_f [GPa]	V_f [%]	L_f [mm]	ϕ_f [mm]
50	210	2.7	13	0.2

Although it is often assumed that the fibers are either unidirectional or randomly dispersed in the cementitious matrix, the actual fiber orientation will

never be unique and the state of anisotropy will depend on the fiber geometry, fiber content and fluid flow properties during the casting phase. In this work we assume a statistical π-periodic Gaussian like probability density function, which is axisymmetric in spherical coordinates:

$$W(\theta) = \frac{w_k \cosh(k\cos(\theta-\theta_0))}{\int_{\varphi=0}^{2\pi}\int_{\theta=0}^{\pi} w_k \cosh(k\cos(\theta-\theta_0))|\sin(\theta)|\,d\theta d\varphi} \quad (36)$$

where $\quad \dfrac{1}{2\pi}\int_{\theta=0}^{\pi}\int_{\varphi=0}^{2\pi} W(\theta,\varphi)|\sin\theta|\,d\theta\,d\varphi = 1$

where $w_k = 2/k\cosh(k)$. Although there is no a physical reason behind the chosen distribution function, one may assume that the axis of symmetry coincide with the average flow direction during the casting phase. The parameters k and θ_0 control, respectively, the degree of uniformity and the angle between the axial symmetric distribution and the crack plane normal direction. Figure 3 shows the distribution function varying the parameter values. Note that the distribution function is uniform when k = 0.
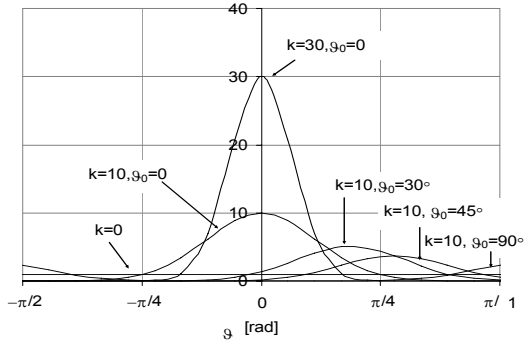
Figure 3. Fiber probability density distribution function for different values of the 2 parameters (k, ϑ_0).

Assuming that the probability distribution *p(z)* of the distance *(z)* between the fiber centroid and the crack plane is uncorrelated from the fiber orientation and uniformly distributed (i.e., $p(z) = 2/L_f$), the composite fiber stress is evaluated by averaging the pull-out force on the crack plane (Lin and Li, 1997), such as

if $[\![\xi]\!] < [\![\xi]\!]^*$

$$\sigma_B([\![\xi]\!]) = \frac{4V_f}{\pi\phi_f}\int_{\vartheta=0}^{\pi/2}\int_{z=0}^{[\![\xi]\!]^0} F_d([\![\xi]\!])\,p(z)\,p(\vartheta)\,dz\,d\vartheta +$$

$$\frac{4V_f}{\pi\phi_f}\int_{\vartheta=0}^{\pi/2}\int_{z=[\![\xi]\!]^0}^{(Lf/2)\cos\vartheta} F_s([\![\xi]\!])\,p(z)\,p(\vartheta)\,dz\,d\vartheta$$

(37)

if $[\![\xi]\!] > [\![\xi]\!]^*$

$$\sigma_B([\![\xi]\!]) = \frac{4V_f}{\pi\phi_f}\int_{\vartheta=0}^{\pi/2}\int_{z=0}^{(Lf/2)\cos\vartheta} F_s([\![\xi]\!])\,p(z)\,p(\vartheta)\,dz\,d\vartheta \quad (38)$$

where the integration limits are properly defined to account *only* for the fiber intercepting the cracks either for the frictional debonding phase or the slip-ping phase. In this simplified approach, the fiber percentage intercepting the crack is the key parameter. Figure 4 shows the fiber percentage intercepting the crack plane in function of the fiber distribution parameters (ϑ_0 and k) as estimated from Eq.(36). It is noticed that a non uniform fiber distribution (i.e., high value of the parameter k) is favorable if oriented towards the crack plane. In other words, the higher the value k, the faster the fiber number decreases with the angle ϑ_0.
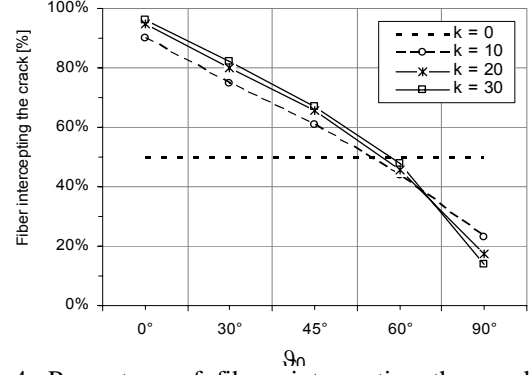
Figure 4. Percentage of fibers intercepting the crack plane varying the parameter (ϑ_0 and k) with respect the loading axis.

Finally, the fiber energy is evaluated by substituting, respectively, Eq. (37) and (38) in the J-Rice line integral of Eq. (8). The dependence of the fiber debonding energy on the fiber distribution (defined by parameters ϑ_0 and k) is shown in Figure 5 for a small crack opening displacement equal to 0.01 mm (i.e., ~$[\![\xi]\!]^*$ of (37)).
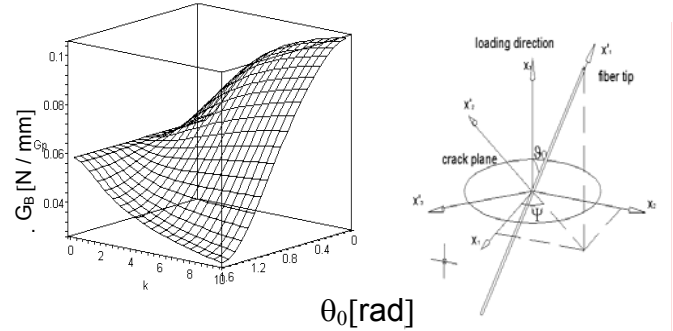
Figure 5. (left) Fiber debonding energy in function of the fiber distribution parameters (ϑ_0 and k) at a crack opening of 0.01 mm; (right) fiber orientation with respect the crack plane.

To explicit the fiber debonding energy G_B as a function of the crack size, we need the crack profile relationship, this is generally obtained by solving an integral function since the crack opening along the crack depends on the fiber bridging stress, which itself depends on the crack opening. For simplicity, we assume that the crack profile takes the same elliptical shape as that for a crack with uniform cohesive traction (i.e., unperturbed by fiber bridging) such as

$$[\![\xi]\!] = \frac{8(1-v^2)}{\pi E}\frac{K_{IC}}{2/\pi f_t\sqrt{\pi a_0}}\sqrt{a^2-r^2} \quad (39)$$

where f_t = tensile strength, ν = Poisson's ratio, r = radial crack coordinate, K_{IC} = critical stress intensity factor (which can be deduced by the fracture energy R_0 by Irwin's relationship). This assumption, which conveniently decouples the crack opening from the bridging stress σ_B, has been often used in literature (Lawn,1993; Leung, 1996), and it can be seen as a first order approximation for small crack opening displacement of the penny shape cracks in the strain hardening regime.

5 MODEL VERIFICATION

The model is calibrated on the experimental direct tensile response of notched specimens drilled out from an L-shaped prototype made of UHPFRC (Figure 6; Toutlemonde *et al.*, 1999). This application is suitable for validating our model since the fiber orientation was found to be strongly oriented due to the casting process (injection) that is represented by a dashed arrow. More precisely, we have specimens "C" drilled along the favorable fiber orientation induced by the casting process, and specimens "A" in the unfavorable orthogonal direction. The crack opening measurement is converted in strain by assuming a measurement length of 50 mm.

The model parameters reported in Table 1 are identified from Toutlemonde *et al.* (1999), while further best fitting parameters are $\tau_u = 4$ MPa and $f_t = 6$ MPa. Figures 7 and 8 show the comparison between the experimental results and the model prediction for a uniaxial tensile test in the two orthogonal direction assuming a strongly localized fiber distribution (i.e., k = 30). In addition, the model predicts the evolution of the material anisotropy and the micromechanics crack parameter, as shown in Figure 9 for the specimens "C". In the same figure, we report the loading function and the stability condition to show that the cracking process is efficiently stabilized by the fiber debonding.

Finally, Figure 10 shows the model sensitivity to the fiber orientation in terms of the material constitutive relationship prediction.
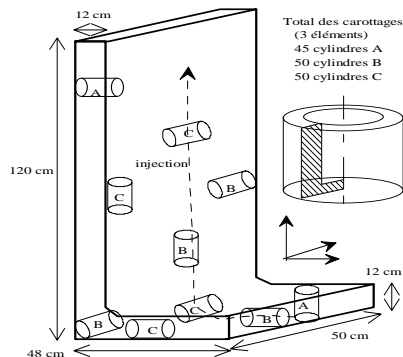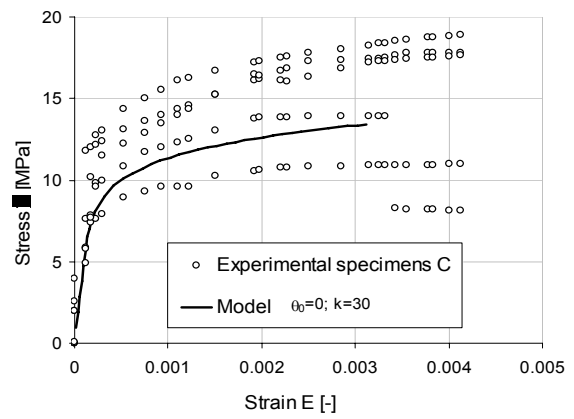

Figure 7. Numerical prediction of the experimental tensile test results for the favorable oriented specimens. "C".
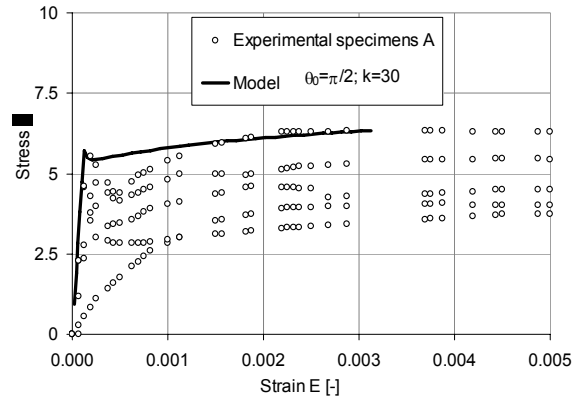

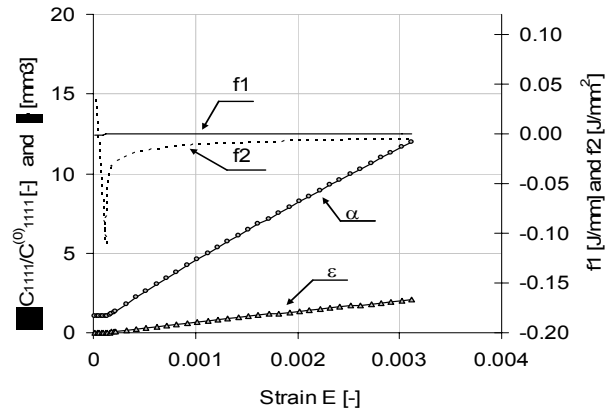Figure 8. Numerical prediction of the experimental tensile test results for the unfavorable oriented specimens "A".

Figure 9. Model prediction of the anisotropy ratio (α), the crack damage parameter, the loading function (f1) of Eq. (10) and the stability condition of Eq. (12) for the specimens "B".
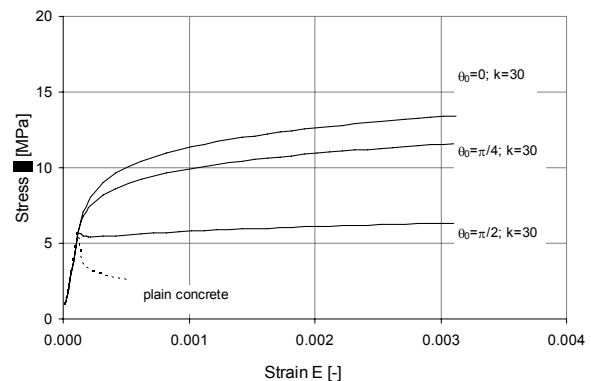

Figure 10. Sensitivity of the constitutive relationship to the fiber orientation.

Figure 6. Specimens drilled out from the nuclear waste container with indication of the main direction of casting flow (dashed arrow).

6 CONCLUDING REMARKS

This work develops a combined fracture-micromechanics model to upscale the UHPFRC material constitutive relation (before crack localization) from the critical microstructure features, such as fiber distribution, fiber-matrix debonding micro mechanism, and initial crack configuration. The approach turns to be a strain formulation of an anisotropic damage model where the homogenized compliance is traced down to the crack density and morphology pattern. The Mori-Tanaka scheme has been used to account for the crack interactions. Two interesting conclusions can be reached:

1. Relative small debonding toughness in UHPFRC (~6 time the fracture energy) are enough to delay the crack localization and allow a ductile strain hardening behavior;

2. The fiber orientation mainly governs the post-cracking ductility up to an extent that, in case of unfavorable distribution, the strain hardening may not occur.

Combined with experimental *in situ* evaluation of the fiber distribution or numerical prediction by flow transport analysis, the model may be used to predict or assess the reliability of UHPFRC post-cracking behavior. Next, the model can be used to identify critical fiber distribution for stability and, after considering mixed fracture mode, to optimize UHPFRC structural applications.

ACKNOWLEDGEMENTS

REFERENCES

Association Francaise de Genie Civil (AFGC) 2002. Ultra High Performance Fibre-Reinforced Concrete, Interim Recommendations, J. Resplendino & J. Petitjean eds.

Bayard, O. & Plé, O., 2003. Fracture mechanics of reactive powder concrete: material modelling and experimental investigations, Engineering Fracture Mechanics 70, 839-851.

Bažant, Z.P. and Planas, J. 1998. Fracture and size effect in concrete and other quasi-brittle materials. Boca Raton, Florida, and London: CRC Press, 616.

Bernier G., Behloul M., 1998 .Effet de l'orientation des fibres sur le comportement des BPR, Revue française de génie civil, 1998, vol. 2, no1, pp. 113-122.

Brian Lawn, 1993. Fracture of brittle solids, Cambridge Solid State Science Series, 378.

Budiansky, B., Hutchinson, J.W., Evans, A.G., 1986. Matrix fracture in fiber-reinforced ceramics. J. Mech. Phys. Solids, 34, 2, 167-189.

Chanvillard, G., Rigaud, S. (2003) Complete characterisation of tensile properties of Ductal® UHPFRC according to the French Recommendations, HPRFCC-4 symposium, Ann Arbor, Michigan, June 16-18.

Chuang,E., Overland, M., Ulm, F.-J. 2001. Length scales of fiber reinforced cementitious composites – a Review. Proc. Fracture Mechanics of Concrete Structures, de Borst *et al.* eds., Lisse, 35-42.

Dormieux, L., Kondo, D., Ulm, F.-J., 2006. A micromechanical analysis of damage propagation in fluid-saturated cracked media. C.R. Mecanique, 334, 440-446.

Eshelby, J. D., 1957, The Determination of the Elastic Field of an Ellipsoidal Inclusion and Related Problems, Proc. R. Soc. London, A241, 376–396.

Karihaloo, B.L., Wang, J., Grzybowski, M., 1996, Double periodic array of bridged cracks and short fiber-reinforcement cementitious composites, J. Mech. Phys. Solids, 44, 10, 1565-1586.

Leung, C.K.Y. & Chi, J. 1995. Crack-bridging force in random ductile fiber brittle matrix composites, J. of Eng. Mech., December, 1315-1324.

Leung, C.K.Y. 1996. Design criteria for pseudoductile fiber-reinforced composites, J. Eng. Mech., January, 10-18.

Li, V. & Leung, C.K.Y. 1992. Theory of steady state and multiple cracking of random discontinuous fiber reinforced composites, ASCE J. of Eng. Mechanics, 2298.

Lin, Z. & and Li, V., 1997. Crack bridging in fiber reinforced cementitious composites with slip-hardening interfaces, J. Mat. Phys. Solids, 45, 5, 763-787.

Marshall, D.B. & Cox, B.N. 1985. The mechanics of matrix cracking in brittle-matrix fiber composites, Acta Metall., 35, 11, 2013-2021.

Mori, T. & Tanaka, K. 1973. Average stress in matrix and average elastic energy of materials with misfitting inclusions, Acta Metall., 21, 571-574.

Rice, J.R. 1968. A path-independent integral and the approximate analysis of strain concentration by notch and cracks, J. Appl. Mech., 35, 379.

Shah, P. & Ouyang, C., 1991. Mechanical Behavior of Fiber-Reinforced Cement-Based Composites, Journal of the American Ceramic Society, 74, 11, 2727-2953.

Tjiptobroto, P., and Hansen, W., 1993, Tensile strain hardening and multiple cracking in high performance cement based composites. ACI Material Journal, 90, 1, Jan.-Feb., 1993.

Toutlemonde, F., Sercombe, J., Torrenti, J.-M., Adeline, R. 1999. Développement d'un conteneur pour l'entreposage de déchets nucléaires : résistance au choc. Revue Française de Génie Civil, vol. 3, n°7-8, 729-756.

Zhang, J. & Li, V.C., 2002. Effect of inclination angle on fiber rupture load in fiber reinforced cementitious composites, Composites Sciences and Technology, 62, 775-781.